IEEE Access
Multidisciplinary | Rapid Review | Open Access Journal

Date of publication xxxx 00, 0000, date of current version xxxx 00, 0000.

Digital Object Identifier 10.1109/ACCESS.2017.Doi Number

Human Presence Sensing and Gesture Recognition for Smart Home Applications with Moving and Stationary Clutter Suppression Using a 60-GHz Digital Beamforming FMCW Radar

PRATEEK NALLABOLU[1], (Student Member, IEEE), ZHANG LI[2], (Student Member, IEEE), HONG HONG[2], (Senior Member, IEEE), AND CHANGZHI LI[1], (Senior Member, IEEE)

[1]Department of Electrical and Computer Engineering, Texas Tech University, Lubbock, TX 79409, USA
[2]School of Electronic and Optical Engineering, Nanjing University of Science and Technology, Nanjing 210094, China

Corresponding author: Prateek Nallabolu (e-mail: prateek-reddy.nallabolu@ttu.edu) and Changzhi Li (changzhi.li@ttu.edu).

This work was supported in part by National Science Foundation under the grant ECCS-1808613 and ECCS-2030094.

ABSTRACT With the advancement of radio frequency (RF) assisted smart home technology, it is critical for the RF sensors deployed indoors to isolate the target of interest from unwanted clutter sources. This paper presents a novel method for suppressing both moving and stationary clutters in an indoor environment to localize stationary human subjects with a millimeter-wave frequency-modulated continuous-wave (FMCW) radar. The method derives its roots from the intrinsic high-pass filter (HPF) characteristic of the exponential moving average (EMA) algorithm, a preferred approach for background stationary clutter suppression. In this work, emphasis was laid on expanding the capability to detect and suppress unwanted moving clutter sources in the indoor environment along with stationary clutters, which has not been widely explored before. The proposed method removes motion artifacts so that the characteristic respiratory signal can be identified for human-aware localization. The paper provides experimental validation of the proposed method, wherein a 60-GHz FMCW radar with digital beamforming (DBF) capability was used to identify the 2-D location of a sitting human subject, with a moving window curtain in the background acting as a strong moving clutter source along with other stationary clutters. In addition, a lateral hand gesture recognition technique is presented, wherein the EMA algorithm was used to enhance the signature of the hand motion. The instantaneous position of the hand at the beginning and end of the gesture was determined to classify the gesture as a left-to-right or right-to-left hand swipe.

INDEX TERMS Exponential moving average (EMA) algorithm, frequency-modulated continuous-wave (FMCW) radar, gesture recognition, human localization, moving clutter suppression, smart homes.

I. INTRODUCTION

Smart homes are emerging residences equipped with a multitude of interactive sensors and internet-connected devices that provide the users an elevated level of comfort, security, and improved energy conservation [1]-[6]. The internet of things (IoT) era has allowed single-point remote access and control to all the appliances in the home. The advancement of various sensor technologies has seen a paradigm shift in smart home technologies from remote access to user-centric context-aware computing.

The user-centric approach relies on human (user) presence sensing and activity recognition to create an ambient intelligent environment [7]-[9]. For example, the detection of human subjects can be used to automatically turn on/off lights, fans, etc. In intelligent heating, ventilation, and air conditioning (HVAC) systems [10], [11], the knowledge of the location and the number of human subjects in an indoor space will be helpful to automatically control the amount of airflow as well as the direction of airflow. Smart homes can assist elderly people and those suffering from cognitive

deficiencies to perform activities of daily living (ADL) [12], [13].

Technologies such as cameras, passive infrared (PIR) sensors, ultrasonic sensors, and radars are the fundamental building blocks of advanced cognitive sensing in smart homes. These sensors are used to detect human subjects and their activities. Camera-based solutions can detect human targets [14], [15], but higher computational cost, sensitivity to ambient light, and privacy concerns limit their deployment. Passive infrared (PIR) sensors and ultrasonic sensors were used for detecting human subjects in [16]-[18]. However, PIR sensors are insensitive to low levels of motion, and ultrasonic sensors require a direct line of sight between the sensor and the occupants. Radars operating in frequency-modulated continuous-wave (FMCW) [19]-[21], frequency-shift keying (FSK) [21]-[23], and ultra-wideband (UWB) [24]-[26] mode have gained significant interests for their ability to alleviate privacy concerns, detect micro motions like human vital signs, and offer through-the-wall detection capabilities.

Clutter removal is a major concern for human presence sensing in modern smart homes. Since there are many clutter sources at home, it is essential to suppress the reflections from strong clutter sources that mask the human target signature. The clutter sources can be broadly classified into stationary and moving clutters. Stationary clutter sources are objects like sofa, table, etc. Moving clutter sources include window curtains, blinds, table fan, etc. With the emphasis on using radars for indoor human presence sensing, a literature review was carried on the existing clutter suppression methods [27]-[39]. Existing works on background clutter suppression using radars concentrated mainly on the removal of stationary clutter. A simple background subtraction technique was used to remove reflections from stationary targets in pulse-Doppler radars [27], strong Tx-Rx leakage in FMCW radars [28], and enable through-the-wall human localization by attenuating the reflections from the wall [29], [30]. By taking advantage of the constant phase response of stationary targets across successive FMCW chirps, a coherent phase difference approach was used to recognize pedestrians in the presence of strong background clutter [31] and distinguishing moving targets from stationary targets [32]. An additional reference antenna was used to remove multi-path clutter by observing the frequency domain correlation between the echo signal and the reference signal captured by the reference antenna [33]. The exponential moving average (EMA) algorithm extracted from the moving target indicator (MTI) was used to remove stationary targets while measuring vital signs and tracking multiple human subjects [34]-[36]. In [37], an adaptive EMA algorithm was proposed for UWB radars to suppress stationary clutter and maintain the signals reflected from a human subject.

However, strong reflections from moving clutter sources can also mask the reflected signals from a human body, thereby failing to detect the presence of a human target. Notable works on moving clutter suppression include segmentation of multiple targets having different Doppler

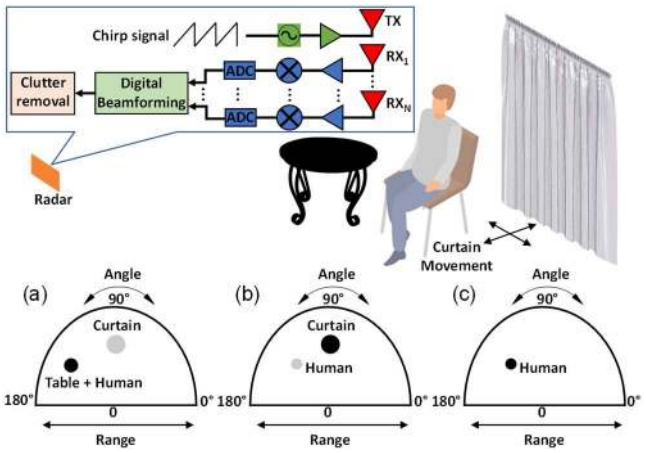

FIGURE 1. **Graphical illustration of the 2-D map of the indoor experiment setup obtained (a) without EMA algorithm, (b) using conventional EMA algorithm, and (c) using the proposed moving clutter suppression method.**

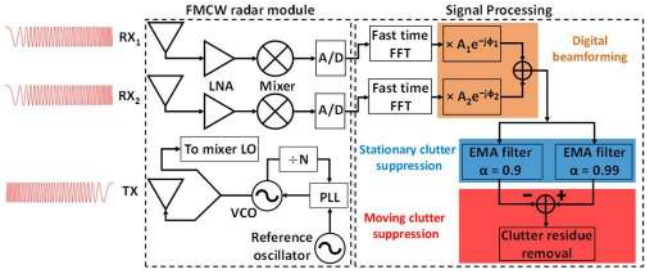

FIGURE 2. **Block diagram of the 60-GHz FMCW radar and a high-level representation of the signal processing flow for the proposed moving clutter suppression method.**

frequencies based on higher-order infinite impulse response (IIR) and finite impulse response (FIR) MTI filters [30]. Nevertheless, higher-order IIR filters are prone to instability, and FIR filters have low computation speed and require large memory. A 2nd-order harmonic radar was proposed to eliminate unwanted moving and stationary clutter information while retaining information from specific targets that can generate non-linear responses [38]. However, the radar requires additional hardware like diplexers and wide bandwidth antennas to capture both fundamental and harmonic responses. An intermodulation radar and a wearable non-linear tag were used to identify stationary human subjects in the presence of strong stationary and moving clutter sources [39]. However, the human subject needs to wear the tag all the time, which can cause discomfort, and the radar receiver chain requires expensive circuitry to filter the echoes from the fundamental frequency tones.

Hand gesture recognition using radar sensors has gained significant interest in the past decade due to the increasing applications of human-machine interaction like gesture-controlled smart TVs, smart homes, and mobile devices. Hand gesture recognition based on Doppler and FMCW radars was discussed in [40]-[46]. Doppler radars rely only on the micro-Doppler analysis, while FMCW radars utilize micro-Doppler

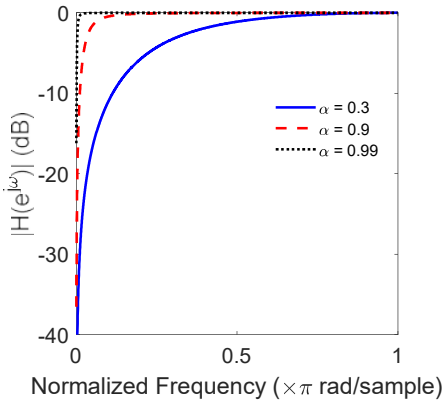

FIGURE 3. Variation of the magnitude response of the EMA filter with the weighting factor *α*.

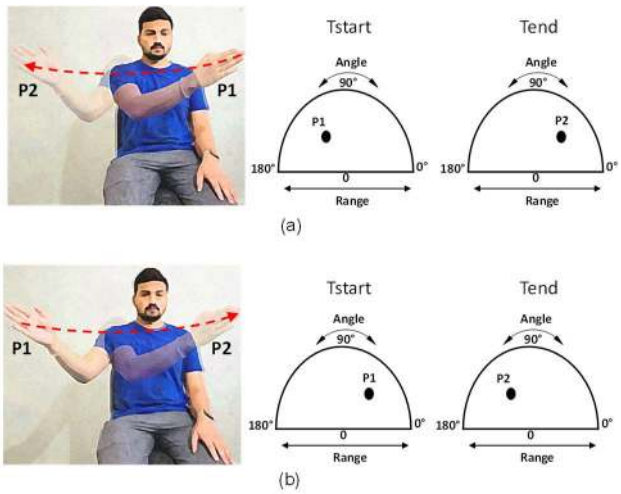

FIGURE 4. Graphical illustration of the lateral hand gesture movement and the 2-D position of the hand at the start and end of the gesture for (a) left-to-right and (b) right-to-left hand swipe.

and range-Doppler processing to classify multiple gestures using machine learning techniques. A challenging case for radars is to extract unique features for hand gestures with similar range-Doppler and time-Doppler characteristics, as in the case of lateral hand motions like left-to-right and right-to-left hand swipe. Although lateral hand gesture detection has been explored in previous works, there are several drawbacks. A 5.8-GHz Doppler radar was employed to classify lateral hand swipe motions based on their micro-Doppler features [40]. However, the speed of the left-to-right and right-to-left hand swipe motions was varied intentionally to avoid generating the same Doppler spectrograms for both the gestures. In [41], a continuous hand motion tracking algorithm was presented using a Doppler radar with one transmitting (Tx) and two receiving (Rx) antennas. However, Doppler radars are highly susceptible to other moving targets in their proximity, whose motion frequencies can overlap with the hand gesture signature. Hand gesture recognition based on 3-D convolutional neural networks (CNN) was proposed in [43], where a 24-GHz FMCW radar with 1Tx-2Rx antenna configuration was used to classify lateral hand sliding motions that exhibited non-identical range trajectories with time. In [44], an FMCW radar with one Tx antenna and four Rx antennas distributed in a 2-D plane was used to classify several gestures, including lateral hand swipe motions.

In this paper, a new approach is devised to suppress not only stationary clutter but also unwanted moving clutter sources in an indoor environment for stationary human target localization using a 60-GHz FMCW radar. By taking advantage of the intrinsic high-pass filter (HPF) nature of the EMA algorithm, filters with different cut-off frequencies are designed by varying the weighting factor α in the EMA algorithm to differentiate between various moving targets in the environment. Using prior knowledge of typical human respiration frequencies, moving targets falling outside the range of these frequencies can be identified as moving clutter sources. The single-input multiple-output (SIMO) configuration of the 60-GHz FMCW radar allows for locating the 2-D position of the human target with the help of digital beamforming. Additionally, a lateral hand gesture detection method aided by the conventional EMA algorithm is proposed, which offers a lower computational cost solution to identify left-to-right and right-to-left hand swipe gestures that have mirrored motions with identical Doppler stamps and minimal radial movement. The EMA filtering helps to suppress the reflections from the human body and enhance the hand gesture signature. The instantaneous 2-D position of the hand is measured at the beginning and end of the gesture using digital beamforming to identify the direction of the hand swipe.

The paper is organized as follows. The theory of the proposed moving clutter suppression method and the lateral hand gesture recognition technique is discussed in Section II. In Section III, the simulation results of the moving clutter suppression method are presented. Experiments conducted to validate the proposed concepts, and the results are discussed in Section IV. Finally, conclusions are drawn in Section V.

II. THEORY

A. MOVING CLUTTER SUPPRESSION

Fig. 1(a) and (b) graphically illustrate the ability of the conventional EMA algorithm to suppress stationary clutter, whereas Fig. 1(c) shows the goal of the proposed method to additionally suppress the unwanted moving clutter and precisely locate the human target using an FMCW radar with digital beamforming capability. A coherent FMCW radar can accurately track the range of a moving target and provide its Doppler information. The mathematical expression for the beat signal $s_b(t)$ generated by an FMCW radar is [19]

$$s_b(t) = \sigma \exp\left(j\left(\frac{4\pi\gamma R(\tau)t}{c} + \frac{4\pi f_c R(\tau)}{c} + \varphi\right)\right), \quad (1)$$

where σ is the amplitude of the baseband signal, γ is the slope of the chirp signal transmitted by the radar, t is the fast-time, $R(\tau)$ is the range evolution of the target along the slow-time τ, f_c is the center frequency of the chirp signal, and c is the speed of light. The slope of the chirp signal is mathematically given as $\gamma = B \times PRF$, where B and PRF represent the bandwidth and chirp repetition frequency of the transmitted chirp signal, respectively. φ is the residual video phase which can be ignored. A fast Fourier transform (FFT) is performed on the beat signal to identify the range of the target, which is represented as

$$s_b(f) = \sigma T \exp\left(j\frac{4\pi f_c R(\tau)}{c}\right) sinc\left(T\left(f - \frac{2\gamma R(\tau)}{c}\right)\right), \quad (2)$$

where T is the duration of each chirp signal, and f is the frequency domain equivalent of the fast-time. To obtain the Doppler information of the targets, the FMCW radar transmits a sequence of chirp signals, referred to as frames. The time-domain data obtained for all the chirps in the frame can be arranged in a 2-D matrix with dimensions $n_{samples} \times n_{chirps}$, where $n_{samples}$ represents the number of samples in each chirp and n_{chirps} represents the number of chirps in a frame. After applying FFT along each row, i.e., fast-time FFT, the frequency-domain data can be represented in a 2-D matrix of size $n_{FFT} \times n_{chirps}$, where n_{FFT} represents the number of points used for performing the FFT operation. Each column of the above frequency-domain matrix can be attributed to a unique range bin, which carries information about targets at that distance in front of the radar. To calculate the Doppler frequencies of the targets, range-Doppler processing is performed by applying FFT along the columns of the frequency-domain matrix, which is referred to as the slow-time FFT. For targets like human subjects that exhibit vital-Doppler motion characteristics, the slow-time phase history $4\pi f_c R(\tau)/c$ is evaluated at the range bin corresponding to the human subject to calculate the vital-sign information.

Fig. 2 represents the 60-GHz FMCW digital beamforming radar architecture along with the proposed moving and stationary clutter removal method. In an indoor environment, the effective beat signal generated by an FMCW radar is the sum of individual beat signals generated due to multiple reflecting sources in the vicinity of the radar. The effective beat signal can be given as

$$r_k(t) = \sum_{i=1}^{L} \sigma_{i,k}[s_b(t)]_{i,k} + n(t), \quad (3)$$

where k is the slow-time index representing the k^{th} chirp in the frame, L is the total number of reflecting sources, and $n(t)$ represents the noise. The beat signals from some of the reflecting sources are unwanted clutter signals, which have to be suppressed.

The EMA algorithm is a first-order FIR filter that calculates the weighted mean of time-series data. The method derives its name due to the exponential decay of the weighting factor for previous data inputs. The EMA algorithm is widely used for stationary clutter suppression due to its ease of implementation and ability to continuously update the background clutter information. The clutter information is updated using the previous clutter data and the instantaneous received signal, which is then used to calculate the clutter-less data. The weighting factor α is used to assign weights to the contribution of the previous clutter data and the instantaneous received signal in calculating the new clutter data.

Mathematically, the background clutter data $c_k(f)$ is calculated as

$$c_k(f) = \alpha c_{k-1}(f) + (1-\alpha) r_k(f), \quad (4)$$

where $0 < \alpha < 1$ and $r_k(f)$ is the FFT output of $r_k(t)$. The clutter-less data $y_k(f)$ is calculated as

$$y_k(f) = r_k(f) - c_k(f). \quad (5)$$

Equation (4) represents a low-pass digital filter (LPF) and (5) represents a high-pass digital filter. The transfer function of the high-pass filter in the z-domain is given as

$$H(z) = \frac{Y(z)}{R(z)} = \frac{\alpha - \alpha z^{-1}}{1 - \alpha z^{-1}}. \quad (6)$$

From (6), it can be observed that the value of α determines the cut-off frequency of the filter. The higher the value of α, the lower is the cut-off frequency. From an FMCW radar point of view, (4) can be understood as a low-pass filter applied across the slow time, which retains the stationary target information. On the other hand, (5) preserves the information of moving targets. As the value of α increases, moving targets with very low motion frequencies can also be identified. Fig. 3 represents the magnitude response of the EMA filter for different α values. It can be observed from Fig. 3 that for lower values of the weighting factor ($\alpha = 0.3$), the cut-off frequency of the EMA filter is high, thereby attenuating stationary targets as well as moving targets with very low Doppler frequency. Conversely, for higher values of the weighting factor ($\alpha = 0.9$, 0.99), the attenuation of slowly-moving targets is significantly reduced while the stationary targets are still suppressed. It should be noted that given the motion frequency of a moving target, the value of α can be chosen accordingly to either retain or suppress the corresponding target information.

The frequency of human respiration falls in the range of 0.1-0.7 Hz. Therefore, the value of α can be set to a higher value to identify a human subject. However, if there are other moving clutter sources in the environment, even those sources would appear in the output of the EMA algorithm. An additional moving clutter suppression step is introduced where the EMA outputs of two different values of α are subtracted to attenuate the unwanted motion frequencies. If the motion frequencies of the stationary human subject (respiration) and the moving clutter source vary largely, the values of α can be chosen accordingly to uniquely locate the human subject in the presence of strong moving clutter. From Fig. 3, it can be noticed that the EMA filters designed with α values of 0.9 and

0.99 can recognize human targets using their inherent respiratory motion and other large Doppler generating clutter. However, the magnitude response of the filters for the above two α values varies vastly at very low frequencies that correspond to the frequency range of the human respiration, while it remains constant for moving clutter with large Doppler frequencies that fall in the passband of the filter. Therefore, by subtracting the filter response calculated using (4) and (5) for α values of 0.9 and 0.99, the signature of the human target gets amplified relative to the signature of the moving clutter.

In specific scenarios, the motion frequency of the moving clutter may fall marginally outside the passband of the EMA filters obtained for weighting factors of 0.9 and 0.99, thereby leading to the slightly different magnitude of the moving clutter echo at the output of the two filters. This mismatch in magnitude retains a very low energy signature of the moving clutter while subtracting the responses of the two filters. To eliminate this residue, additional signal processing is performed by observing the signal strength of the echoes for α = 0.9 and 0.99 EMA filters. The difference in the moving clutter echo signal strength is minimal for the above-mentioned EMA filters, whereas the human echo would have a larger difference. If the signal strength ratio lies below a certain threshold, the echo can be identified as the moving clutter residue and then suppressed. The threshold is chosen as the ratio of the magnitude response of the α = 0.99 and 0.9 EMA filters at 8 Hz, which is significantly higher than the characteristic respiration frequency of a human subject. This assumes that the moving clutter has at least such a high motion frequency.

The proposed moving clutter suppression step is applied across all the range bins, thus suppressing stationary and moving clutter information at every range. To calculate the angular information of the target, digital beamforming technique is employed. In this method, the generated baseband responses from multiple receiving antennas are multiplied with corresponding complex weights, then summed to extract the target information along an azimuth direction θ. This is equivalent to physically steering the antenna beam towards the azimuth angle θ using the analog beamforming method. The complex weights (a_m) can be represented as a combination of amplitude (A_m) and phase (ϕ_m) weights. To obtain the target information along θ using a uniformly spaced 1-D antenna array, the amplitude weight for each antenna element is kept constant (normalized to unity), and a progressive phase shift is applied across consecutive antenna elements. To digitally steer the beam along the azimuth direction θ using an FMCW radar with n_{RX} receiving antenna elements, the corresponding complex weights for each antenna element can be calculated as:

$$a_m = A_m e^{-j\phi_m},\ A_m = 1,\ \phi_m = \frac{2\pi(m-1)d\cos\phi}{\lambda},\quad m = 1,2,\ldots,n_{RX}, \tag{7}$$

where d is the spacing between the antenna elements and λ is the wavelength in air calculated at the center frequency f_c.

The flow to differentiate the human subject from moving clutter can be realized in detail using the following steps.

1. Using the SIMO configuration of the FMCW radar, the received signals across multiple antennas after FFT processing along the fast time can be represented using an array $D[n_{chirps} \times n_{FFT} \times n_{RX}]$.
2. For each steering angle $\theta \in \theta_N$ along the azimuth direction, perform digital beamforming operation on each slow time data instance of D to get the target information E_θ $[n_{chirps} \times n_{FFT}]$ along θ direction, prior to applying the EMA algorithm. θ_N represents the entire set of steering angles along the azimuth direction.
3. For each $\alpha \in [0.9, 0.99]$, calculate the clutter-less data using (5) for each steering angle θ. Perform the mean of the absolute values along the slow time for the computed data. Place the obtained clutter-less data for all the steering angles into a matrix $E(\alpha)$, whose size is given by $\theta_N \times n_{FFT}$. $E(\alpha)$ represents the clutter-less 2-D map data for a given α.
4. Calculate $E(0.99) - E(0.9)$ to get the 2-D map data with a strong human target signature along with the moving clutter residue. To remove the clutter residue, identify the location of the data points whose magnitude ratio ($E(0.99)/E(0.9)$) is below a certain threshold along each row of the above-calculated 2-D map data, and replace their corresponding magnitudes with the least data point magnitude in that row. The resulting 2-D data contains only the echo of the human target.

B. LATERAL HAND GESTURE RECOGNITION

Fig. 4(a) and (b) illustrate the left-to-right and right-to-left lateral hand gestures, respectively. P1 and P2 represent the position of the hand at the start and end of the gesture. A novel approach to distinguish the above-mentioned hand gestures is devised, where a SIMO FMCW radar with beamforming capabilities is used to determine the instantaneous 2-D position of the hand at the start and end of the gesture.

However, the radar cross-section of the hand is very small, and the reflections from the human subject can mask the signature of the hand movement. Since the Doppler frequencies of the hand gesture and the human vital signs vary considerably, the conventional EMA filter with a weighting factor of 0.3 is used to suppress the reflections from the human body and retain the signature of the hand movement. This additionally filters the reflections from any stationary objects nearby. The EMA filtering is applied to the recorded slow-time data for all the n_{RX} receiving antennas after performing FFT. The start and end timestamps of the hand gesture are measured from the filtered data. Digital beamforming is then applied to the data corresponding to the start and end timestamps to locate the instantaneous 2-D position of the

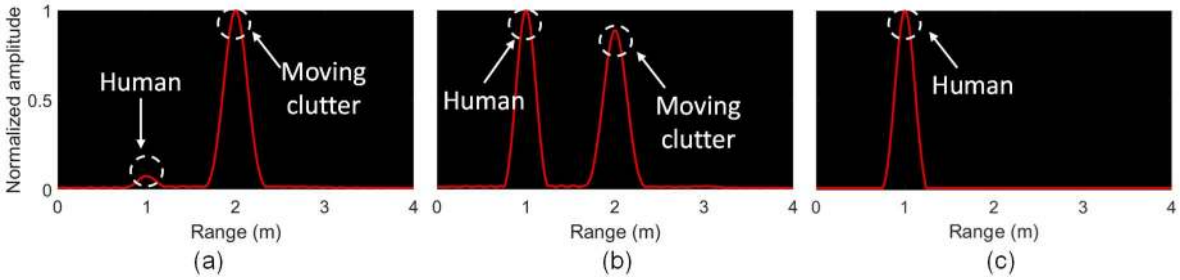

FIGURE 5. Simulation results demonstrating the high-pass filter nature of the conventional EMA algorithm for α value of (a) 0.5 and (b) 0.99. (c) Suppression of stationary and moving clutters using the proposed moving clutter suppression method.

hand. If the shift in the angular position of the hand is clockwise, the hand motion can be recognized as a left-to-right hand swipe, whereas the right-to-left hand swipe would create an anti-clockwise shift in the angular position of the hand.

III. SIMULATION

To initially verify the effectiveness of the proposed moving clutter suppression method, simulations were carried out in MATLAB software. The FMCW chirp signal was configured to have a bandwidth of 1 GHz and a chirp duration of 64 μs. A total of 16000 chirps were considered with a pulse repetition frequency of 806.67 Hz. The sampling rate was set to 1 MHz. The key FMCW parameters are listed in Table I. A human target with a vital-Doppler frequency of 0.4 Hz, a moving clutter with a Doppler frequency of 20 Hz, and a stationary target were assumed as reflecting sources at a distance of 1 m, 2 m, and 3 m, respectively, from the radar. It should be noted that the sampling frequency along the slow-time is equal to the pulse repetition frequency. For the above-mentioned parameters, the radar can detect moving targets with a maximum Doppler frequency of 403.33 Hz.

To demonstrate the effect of the weighting factor α on the outcome of the EMA algorithm, two different values, 0.5 and 0.99, were considered. For α = 0.5, the stationary and human targets were highly suppressed, while the moving clutter signature was strong, as shown in Fig. 5(a). For α = 0.99, the stationary target was highly suppressed, whereas the human target and the moving clutter had strong peaks, as shown in Fig. 5(b). From Fig. 5(b), it can be observed that the conventional EMA algorithm retains the moving clutter signature. To completely suppress the signature of the moving clutter, the proposed method was simulated using α values of 0.99 and 0.9. For α = 0.9, the 3-dB cut-off frequency of the filter was 13 Hz. The normalized magnitude response of the filter was -30dB at 0.4 Hz and -0.2 dB at 20 Hz. Similarly, for α = 0.99, the equivalent EMA filter had a cut-off frequency of 1.24 Hz with a normalized magnitude response of -10 dB at 0.4 Hz and -0.002 dB at 20 Hz. Upon subtracting the two filter responses, the signature of the moving clutter source was highly suppressed while that of the human subject was relatively boosted. A magnitude ratio threshold of two (linear scale) was considered to eliminate the moving clutter residue. This threshold value was the ratio of the magnitude response of α = 0.99 and 0.9 EMA filters at 8 Hz frequency for the above-mentioned radar parameters. Fig. 5(c) shows the obtained result where both the stationary and moving clutter sources were totally suppressed.

IV. EXPERIMENTS

A. MOVING CLUTTER SUPPRESSION

For experimental validation, the FMCW radar chip *BGT60TR13C* from Infineon Technologies AG shown in the inset of Fig. 6 was used. The radar chip can provide a full-scale bandwidth of 5-GHz. The radar has one transmitting antenna (Tx) and three receiving antennas (Rx1, Rx2, and Rx3). The three receiving antennas are placed in an L-shape to provide beamforming capabilities along the azimuth and elevation directions, as shown in the inset in Fig. 6. In this experiment, two receiving antennas (Rx2 and Rx3) were used to perform digital beamforming along the azimuth direction. The FMCW parameters used for the experiments are listed in Table I. The experiments were conducted in an indoor environment. A moving window curtain was used as the source of moving clutter because it is one of the most common sources of moving clutter in office spaces, living rooms, and bed spaces. A table fan placed inside the closet, as shown in Fig. 6, was used to move the curtain located at 1.8m and 90°. The curtain has an aperiodic and random motion, with motion frequency varying between 10 Hz and 200 Hz. A human subject was seated at 1m and 120° relative to the radar position. The experimental setup also consists of stationary clutter sources, including a mirror and a wall.

Fig. 7(a) represents the 2-D map of the experimental space before applying the EMA algorithm. It is clear from Fig. 7(a) that the location of the human subject cannot be uniquely identified. The strong clutter sources mask the human body signature. Fig. 7(b) and 7(c) represent the human localization results using the conventional EMA algorithm and the proposed moving clutter suppression method, respectively. The data for Fig. 7(b) was obtained using the conventional EMA algorithm with an α value of 0.99. The signature of the curtain is illustrated, which could be misinterpreted as a human subject. Further, ghost targets were observed in Fig. 7(b) due to possible multiple reflections between the wall and the curtain, creating ghost images of the curtain at a farther

TABLE I
KEY FMCW RADAR PARAMETERS

	Clutter suppression	Hand gesture recognition
Chirp start frequency	60 GHz	60 GHz
Chirp stop frequency	61 GHz	60.5 GHz
Bandwidth	1 GHz	500 MHz
Samples per chirp	64	64
Sampling frequency	1 MHz	1 MHz
Chirp time	64 µs	64 µs
Chirp repetition rate	806.67 Hz	806.67 Hz
Chirps per frame	16	16
Number of frames	1000	200
Number of active receiver channels	2	2

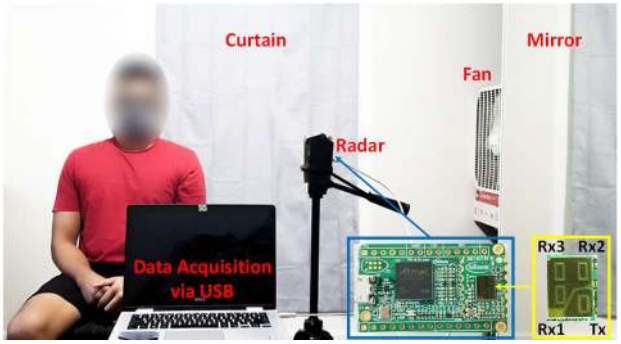

FIGURE 6. Experiment setup for background moving and stationary clutter suppression. (Inset: radar module and its antenna configuration)

range. Since the ghost targets have the same Doppler characteristics as the curtain, they would also be suppressed using the proposed method. It is evident from Fig. 7(c) that the 2-D location of the human subject could be uniquely identified using the proposed method that was able to effectively suppress the signature of the curtain, its ghost images, and most of the curtain residue. The magnitude ratio threshold was chosen as two for these measurement results. The leftover curtain residue appears due to the poor angular resolution provided by the 60-GHz FMCW radar, which offers only two receiving channels for digital beamforming. It should be noted that there was no residue at the true angular location of the curtain, which verifies the effectiveness of the proposed method.

In a different experiment scenario shown in Fig. 8(a), the table fan was used as the moving clutter source. Comparing Fig. 8(b) and (c), it can be noticed that the signature of the fan was suppressed without any ghost targets. The above two experiments verify the 2-D human localization capability of the proposed method in the presence of a window curtain/table fan acting as a moving clutter and other stationary clutter sources, including the wall, sofa, and mirror. It also demonstrates the advantage of the proposed algorithm over the conventional EMA to suppress unwanted moving clutters.

In the 2-D map results presented in Fig. 7 and Fig. 8, it can be observed that the echoes of the targets are spread out in the angular axis. The effective 3-dB beamwidth of an antenna

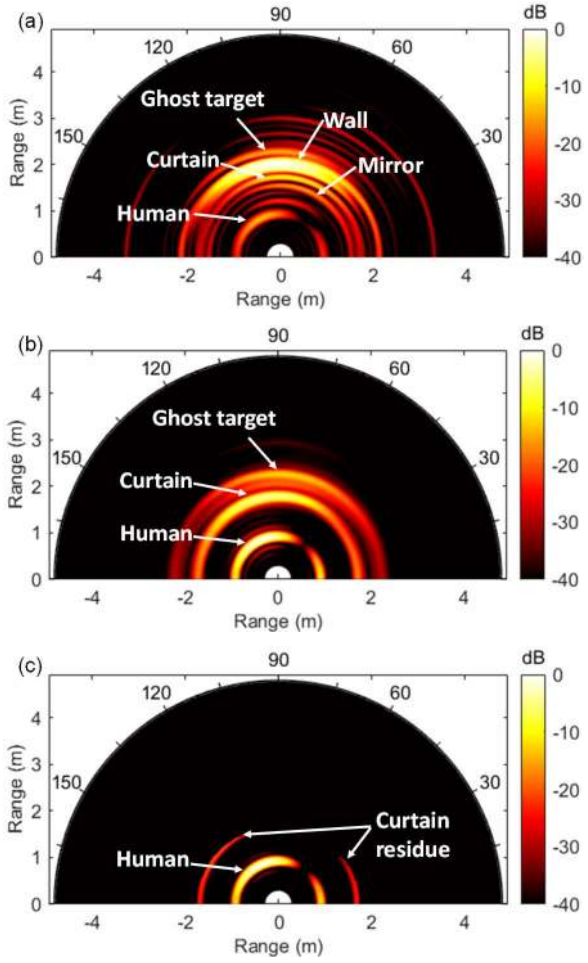

FIGURE 7. Experiment results obtained (a) without applying EMA, (b) using the conventional EMA algorithm, and (c) using the proposed moving clutter suppression method.

array depends on the number of elements in the array. Since the 60-GHz FMCW radar provides only two antenna channels (Rx2, Rx3) for beamforming along the azimuth, it offers a large beamwidth, thereby causing the target echoes to appear as wide arcs in the 2-D map plots. However, the signal strength of the arc is the highest at the true angular location of the targets, as evident from Fig. 7(c), where the echo of the human subject has the highest energy signature at 120°. In general, the proposed clutter removal method is applicable to systems with more antenna channels to achieve better 3-dB beamwidth and completely remove any moving clutter residue.

B. LATERAL HAND GESTURE RECOGNITION

Experiments were conducted using the same radar chirp *BGT60TR13C* to validate the proposed lateral hand gesture recognition method. A human subject seated at 1.5 m and 90° in front of the radar was performing the gestures illustrated in Fig. 4. The FMCW parameters for this experiment are mentioned in Table I. The receiving antennas Rx2 and Rx3 were turned on to enable digital beamforming along the azimuth.

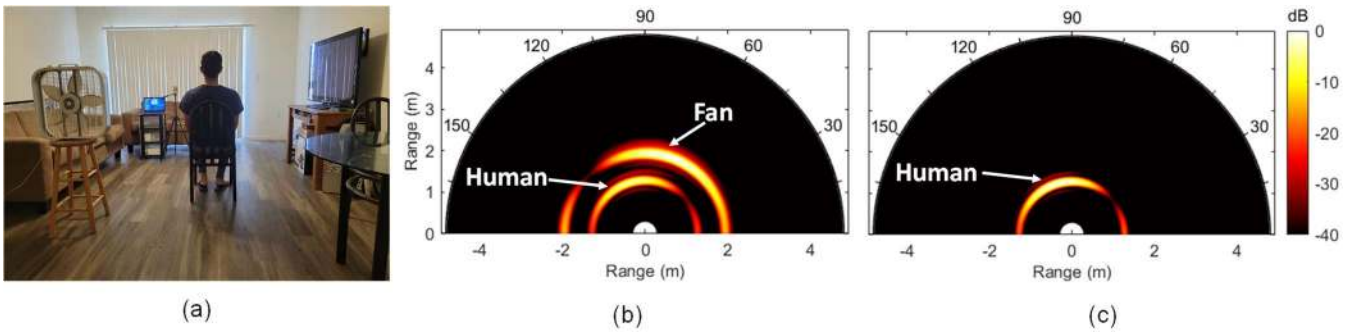

FIGURE 8. **(a) Experiment setup using a table fan as moving clutter source. The obtained 2-D maps using (b) conventional EMA algorithm and (c) proposed moving clutter suppression method.**

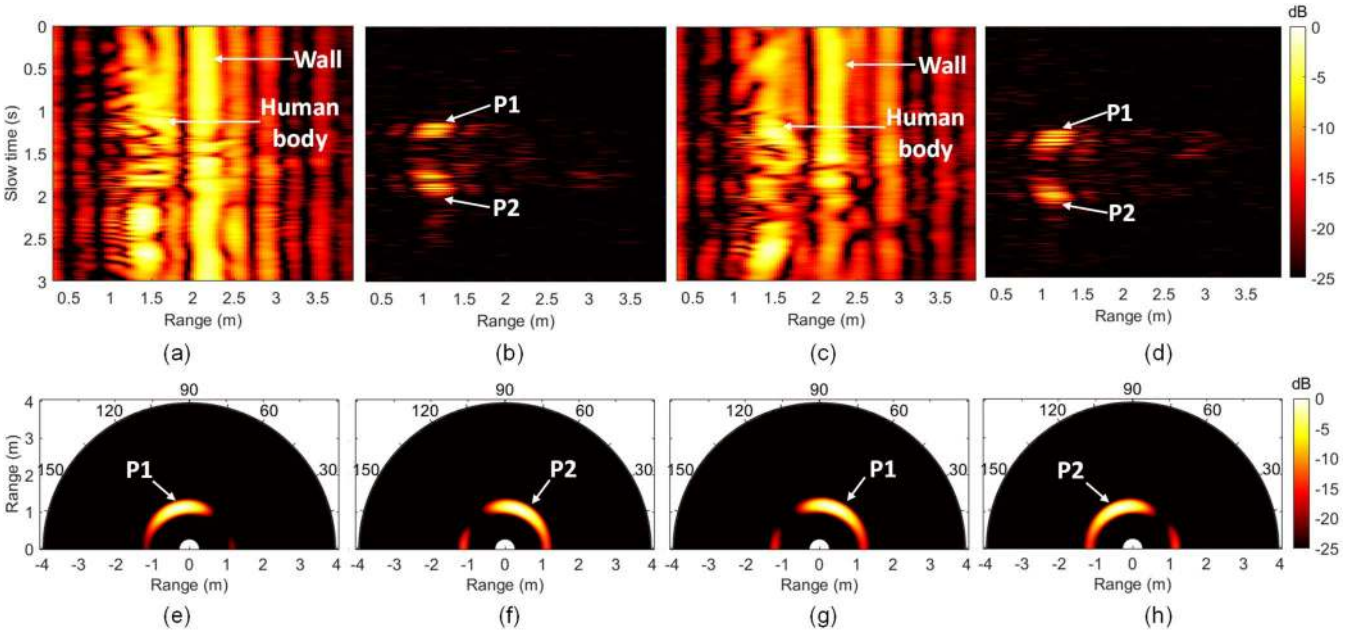

FIGURE 9. **The slow-time range maps for the left-to-right hand swipe: (a) before and (b) after applying EMA filtering, and the right-to-left hand swipe: (c) before and (d) after applying EMA filtering. The instantaneous 2-D position of the hand at the: (e) start and (f) end of left-to-right lateral hand gesture, (g) start and (h) end of right-to-left hand gesture.**

In the first scenario, the human subject performed the left-to-right swipe. Fig. 9(a) shows the obtained slow-time range map for Rx3 antenna data prior to EMA filtering. It can be observed that the strong reflections from the human body completely overwhelm the hand gesture signature. After applying EMA filtering with $\alpha = 0.3$, the reflections from the human body and the wall were filtered, as shown in Fig. 9(b). The value of α was chosen such that the human body reflections were highly suppressed without filtering the hand gesture signature. While performing the gesture, the hand of the human subject extends around 0.3 m away from the body. For a human seated at 1.5 m, the hand motion signature should be around 1.2 m, which was observed in Fig. 9(b). The start and end timestamps of the gesture were measured as 1.1 s and 2 s. The digital beamforming results at these timestamps shown in Fig. 9(e) and (f) indicate a clockwise shift in the angular position of the hand, thereby confirming the theory presented in Section II-B. With a similar setup, the human subject performed the right-to-left hand swipe. The slow-time range maps before and after applying the EMA filtering are shown in Fig. 9(c) and (d). With the start and end timestamps measured as 1.2 s and 2.1 s, the 2-D maps in Fig. 9(g) and (h) indicate an anti-clockwise shift in the instantaneous position of the hand. Comparison between the existing and proposed lateral hand swipe recognition techniques is summarized in Table II.

A small gap in the hand gesture signature can be observed in Fig. 9(b) and (d). This occurs when the hand is precisely in front of the radar during the gesture. In this instance, the reflections from the hand are very minimal, creating a slight discontinuity in the hand gesture signature. Since the angular resolution of the radar is limited, the hand motion was performed with a larger lateral displacement to demonstrate the shift in the hand position. When radars with a higher number of antenna channels are used, lateral hand gestures with smaller displacements can also be easily recognized. The instantaneous 2-D position of the hand can be integrated as a new feature to existing machine learning techniques that are

TABLE II
COMPARISON OF RELEVANT LATERAL HAND SWIPE RECOGNITION WORKS

Previous Works	Sensor Type	Number of Tx/Rx elements	Lateral hand swipe recognition	Immune to surrounding moving clutter
[40]	Doppler	1/1	No	No
[41]	Doppler	1/2	Yes	No
[43]	FMCW	1/2	No	Yes
[44]	FMCW	1/4	Yes	Yes
This work	FMCW	1/2	Yes	Yes

already trained to classify multiple gestures, allowing them to identify the above-mentioned hand swipe motions.

V. CONCLUSION

Measurements from a millimeter-wave digital beamforming radar were processed using the EMA algorithm with different α values, then combined to suppress both moving and stationary clutter sources to successfully locate stationary human subjects in an indoor environment. The proposed method was developed by exploring the unique frequency response of the EMA algorithm and assuming that the dynamics of the moving clutter source are different from human respiration with periodic characteristics. Experimental results were presented to demonstrate the ability of the proposed method to uniquely identify the 2-D location of a human subject in a highly cluttered environment composed of a moving window curtain and other stationary clutters. Utilizing the 1Tx-2Rx antenna configuration of the 60-GHz radar, a cost-effective solution to classify the direction of lateral hand motion was proposed by employing EMA filtering in conjunction with digital beamforming. The EMA algorithm was used to boost the signature of the hand motion and attenuate the strong reflections from the human body and other stationary clutter sources in the vicinity, while the direction of lateral hand motion was identified by tracking the 2-D position of the hand using digital beamforming. Future work includes exploring higher-order EMA filters and addressing the limitations of the current approach, which include suppressing moving clutter sources with motion patterns closer to the respiration of the human subject.

ACKNOWLEDGMENT

The authors would like to thank Infineon Technologies AG for providing the millimeter-wave radar modules.

REFERENCES

[1] M. R. Alam, M. B. I. Reaz, and M. A. M. Ali, "A Review of Smart Homes—Past, Present, and Future," in *IEEE Transactions on Systems, Man, and Cybernetics, Part C* (*Applications and Reviews*), vol. 42, no. 6, pp. 1190-1203, Nov. 2012.

[2] M. Chan, D. Estève, C. Escriba, and E. Campo, "A review of smart homes—Present state and future challenges," *Comput. Methods Programs Biomed*., vol. 91, no. 1, pp. 55–81, 2008.

[3] L. C. De Silva, C. Morikawa, and I. M. Petra, "State of the art smart homes," *Engineering Applications of Artificial Intelligence*, vol. 25, no. 7, pp. 1313-1321, 2012.

[4] M. Khan, B. N. Silva, and K. Han, "Internet of Things Based Energy Aware Smart Home Control System," in *IEEE Access*, vol. 4, pp. 7556-7566, 2016.

[5] H. Jiang, C. Cai, X. Ma, Y. Yang, and J. Liu, "Smart Home Based on WiFi Sensing: A Survey," in *IEEE Access*, vol. 6, pp. 13317-13325, 2018.

[6] S. U. Jan, S. Ahmed, V. Shakhov, and I. Koo, "Toward a Lightweight Intrusion Detection System for the Internet of Things," in *IEEE Access*, vol. 7, pp. 42450-42471, 2019.

[7] L. Chen, C. D. Nugent, and H. Wang, "A Knowledge-Driven Approach to Activity Recognition in Smart Homes," in *IEEE Transactions on Knowledge and Data Engineering*, vol. 24, no. 6, pp. 961-974, June 2012.

[8] C. Debes, A. Merentitis, S. Sukhanov, M. Niessen, N. Frangiadakis and, A. Bauer, "Monitoring Activities of Daily Living in Smart Homes: Understanding human behavior," in *IEEE Signal Processing Magazine*, vol. 33, no. 2, pp. 81-94, March 2016.

[9] A. Yassine, S. Singh, and A. Alamri, "Mining Human Activity Patterns From Smart Home Big Data for Health Care Applications," in *IEEE Access*, vol. 5, pp. 13131-13141, 2017.

[10] H. Mirinejad, K. C. Welch, and L. Spicer, "A review of intelligent control techniques in HVAC systems," *2012 IEEE Energytech*, Cleveland, OH, USA, 2012, pp. 1-5.

[11] K. Chinnakani, A. Krishnamurthy, J. Moyne, A. Arbor, and F. Gu, "Comparison of energy consumption in HVAC systems using simple ON-OFF, intelligent ON-OFF and optimal controllers," *2011 IEEE Power and Energy Society General Meeting*, Detroit, MI, USA, 2011, pp. 1-6.

[12] H. Ghayvat, J. Liu, S. C. Mukhopadhyay, and X. Gui, "Wellness Sensor Networks: A Proposal and Implementation for Smart Home for Assisted Living," in *IEEE Sensors Journal*, vol. 15, no. 12, pp. 7341-7348, Dec. 2015.

[13] J. Rafferty, C. D. Nugent, J. Liu, and L. Chen, "From Activity Recognition to Intention Recognition for Assisted Living Within Smart Homes," in *IEEE Transactions on Human-Machine Systems*, vol. 47, no. 3, pp. 368-379, June 2017.

[14] Y. Sun, W. Meng, C. Li, and X. Wu, "Panoramic Camera-Based Human Localization Using Automatically Generated Training Data," in *IEEE Access*, vol. 8, pp. 48836-48845, 2020.

[15] D. Ding, R. A. Cooper, P. F. Pasquina, and L. Fici-Pasquina, ''Sensor technology for smart homes,'' *Maturitas*, vol. 69, no. 2, pp. 131–136, June 2011.

[16] B. Yang, Y. Lei, and B. Yan, "Distributed Multi-Human Location Algorithm Using Naive Bayes Classifier for a Binary Pyroelectric Infrared Sensor Tracking System," in *IEEE Sensors Journal*, vol. 16, no. 1, pp. 216-223, Jan. 2016.

[17] C. G. Raghavendra, S. Akshay, P. Bharath, M. Santosh, and D. Vishwas, "Object tracking and detection for short range surveillance using 2D ultrasonic sensor array," *2016 International Conference on Circuits*, *Controls*, *Communications and Computing* (*I4C*), Bangalore, 2016, pp. 1-4.

[18] Sonia, A. M. Tripathi, R. D. Baruah, and S. B. Nair, "Ultrasonic sensor-based human detector using one-class classifiers," *2015 IEEE International Conference on Evolving and Adaptive Intelligent Systems* (*EAIS*), Douai, France, 2015, pp. 1-6.

[19] Z. Peng et al., "A Portable FMCW Interferometry Radar With Programmable Low-IF Architecture for Localization, ISAR Imaging, and Vital Sign Tracking," in *IEEE Transactions on Microwave Theory and Techniques*, vol. 65, no. 4, pp. 1334-1344, April 2017.

[20] Z. Peng, L. Ran, and C. Li, "A K -Band Portable FMCW Radar With Beamforming Array for Short-Range Localization and Vital-Doppler Targets Discrimination," *in IEEE Transactions on Microwave Theory and Techniques*, vol. 65, no. 9, pp. 3443-3452, Sept. 2017.

[21] C. Li, J. Wang, D. Rodriguez, A. Mishra, Z. Peng, and Y. Li, "Portable Doppler/FSK/FMCW Radar Systems for Life Activity Sensing and Human Localization," *2019 14th International Conference on Advanced Technologies, Systems and Services in Telecommunications* (*TELSIKS*), Nis, Serbia, 2019, pp. 83-93.

[22] A. Mishra, W. McDonnell, J. Wang, D. Rodriguez, and C. Li, "Intermodulation-Based Nonlinear Smart Health Sensing of Human Vital Signs and Location," in *IEEE Access*, vol. 7, pp. 158284-158295, 2019.

[23] J. Wang, D. Rodriguez, A. Mishra, P. R. Nallabolu, T. Karp, and C. Li, "24-GHz Impedance-Modulated BPSK Tags for Range Tracking and Vital Signs Sensing of Multiple Targets Using an FSK Radar," in *IEEE Transactions on Microwave Theory and Techniques*, Jan. 2021.

[24] A. G. Yarovoy, L. P. Ligthart, J. Matuzas, and B. Levitas, "UWB radar for human being detection," in *IEEE Aerospace and Electronic Systems Magazine*, vol. 21, no. 3, pp. 10-14, March 2006.

[25] S. Chang, N. Mitsumoto, and J. W. Burdick, "An algorithm for UWB radar-based human detection," *2009 IEEE Radar Conference*, Pasadena, CA, USA, 2009, pp. 1-6.

[26] J. W. Choi, S. S. Nam, and S. H. Cho, "Multi-Human Detection Algorithm Based on an Impulse Radio Ultra-Wideband Radar System," in *IEEE Access*, vol. 4, pp. 10300-10309, 2016.

[27] Y. Wang, Q. Liu, and A. E. Fathy, "CW and Pulse–Doppler Radar Processing Based on FPGA for Human Sensing Applications," in *IEEE Transactions on Geoscience and Remote Sensing*, vol. 51, no. 5, pp. 3097-3107, May 2013.

[28] S. Häfner, A. Dürr, C. Waldschmidt, and R. Thomä, "Mitigation of Leakage in FMCW Radars by Background Subtraction and Whitening," in *IEEE Microwave and Wireless Components Letters*, vol. 30, no. 11, pp. 1105-1107, Nov. 2020.

[29] L. Qiu, T. Jin, J. Zhang, B. Lu, and Z. Zhou, "An iterative singular vector decomposition based micro-motion target indication in through-the-wall radar," *2016 IEEE International Geoscience and Remote Sensing Symposium* (*IGARSS*), 2016, pp. 6597-6600.

[30] M. Ash, M. Ritchie, and K. Chetty, "On the Application of Digital Moving Target Indication Techniques to Short-Range FMCW Radar Data," in *IEEE Sensors Journal*, vol. 18, no. 10, pp. 4167-4175, May 2018.

[31] E. Hyun, Y.-S. Jin, and J.-H. Lee, "A pedestrian detection scheme using a coherent phase difference method based on 2D range-Doppler FMCW radar," *Sensors*, vol. 16, no. 1, p. 124, 2016.

[32] E. Hyun, Y. Jin, and J. Lee, "Moving and stationary target detection scheme using coherent integration and subtraction for automotive FMCW radar systems," *2017 IEEE Radar Conference* (*RadarConf*), 2017, pp. 0476-0481.

[33] D. Zhao, J. Wang, G. Chen, J. Wang, and S. Guo, "Clutter Cancellation Based on Frequency Domain Analysis in Passive Bistatic Radar," in *IEEE Access*, vol. 8, pp. 43956-43964, 2020.

[34] A. Lazaro, D. Girbau, and R. Villarino, "Techniques for clutter suppression in the presence of body movements during the detection of respiratory activity through UWB radars," *Sensors 2014*, vol. 14, no. 2, pp. 2595-2618, Feb. 2014.

[35] Z. Duan and J. Liang, "Non-Contact Detection of Vital Signs Using a UWB Radar Sensor," in *IEEE Access*, vol. 7, pp. 36888-36895, 2019.

[36] C. Will, P. Vaishnav, A. Chakraborty, and A. Santra, "Human Target Detection, Tracking, and Classification Using 24-GHz FMCW Radar," in *IEEE Sensors Journal*, vol. 19, no. 17, pp. 7283-7299, Sept. 2019.

[37] B. Lee, S. Lee, Y. Yoon, K. Park, and S. Kim, "Adaptive clutter suppression algorithm for human detection using IR-UWB radar," *2017 IEEE SENSORS*, Glasgow, United Kingdom, 2017, pp. 1-3.

[38] K. A. Gallagher, R. M. Narayanan, G. J. Mazzaro, K. I. Ranney, A. F. Martone, and K. D. Sherbondy, "Moving target indication with non-linear radar," *2015 IEEE Radar Conference* (*RadarCon*), 2015, pp. 1428-1433.

[39] A. Mishra and C. Li, "A Low Power 5.8-GHz ISM-Band Intermodulation Radar System for Target Motion Discrimination," in *IEEE Sensors Journal*, vol. 19, no. 20, pp. 9206-9214, Oct. 2019.

[40] Y. Kim and B. Toomajian, "Hand Gesture Recognition Using Micro-Doppler Signatures With Convolutional Neural Network," in *IEEE Access*, vol. 4, pp. 7125-7130, 2016.

[41] T. Fan et al., "Wireless Hand Gesture Recognition Based on Continuous-Wave Doppler Radar Sensors," in *IEEE Transactions on Microwave Theory and Techniques*, vol. 64, no. 11, pp. 4012-4020, Nov. 2016.

[42] S. Skaria, A. Al-Hourani, M. Lech, and R. J. Evans, "Hand-Gesture Recognition Using Two-Antenna Doppler Radar With Deep Convolutional Neural Networks," in *IEEE Sensors Journal*, vol. 19, no. 8, pp. 3041-3048, April 2019.

[43] Z. Zhang, Z. Tian, and M. Zhou, "Latern: Dynamic Continuous Hand Gesture Recognition Using FMCW Radar Sensor," in *IEEE Sensors Journal*, vol. 18, no. 8, pp. 3278-3289, April 2018.

[44] S. Ryu, J. Suh, S. Baek, S. Hong, and J. Kim, "Feature-Based Hand Gesture Recognition Using an FMCW Radar and its Temporal Feature Analysis," in *IEEE Sensors Journal*, vol. 18, no. 18, pp. 7593-7602, Sept. 2018.

[45] J. Lien, N. Gillian, M. E. Karagozler, P. Amihood, C. Schwesig, E. Olson, H. Raja, I. Pouryrev, and G. Atap, "Soli: Ubiquitous gesture sensing with millimeter wave radar," *ACM Trans*. *Graph*. *Artic*., vol 35, no. 10, Oct. 2016.

[46] D. V. Q. Rodrigues and C. Li, "Hand gesture recognition using FMCW radar in multi-person scenario," in *Proc*. *IEEE MTT-S Radio and Wireless Symposium* (*RWS*), 2021 (to be published).

Prateek Nallabolu (S'18) received the B.Tech. degree in electronics and communications engineering from Jawaharlal Nehru Technological University, Hyderabad, India, in 2016, and the M.S. degree in electrical engineering from Texas Tech University in 2018. He is currently pursuing a Ph.D. degree at Texas Tech University, Lubbock, TX, USA.

His research interests include microwave circuits and systems, wireless RF sensors, and automotive radar security.

Li Zhang (S'21) received the B.S. degree from the Nanjing University of Science and Technology, Nanjing, China, in 2015, where he is currently pursuing the Ph.D. degree. In 2019, he was a visiting scholar with the department of Electrical and Computer Engineering in Texas Tech University, Lubbock, United States.

His current research interests include radar signal processing, computer vision and machine learning of biomedical application.

Hong Hong (M'10-SM'20) received the Ph.D. degree in electrical engineering from Nanjing University, Nanjing, China, in 2010. He is currently an associate professor in School of Electronic and Optical Engineering, Nanjing University of Science and Technology, Nanjing, China. His current research interests include biomedical applications of microwave technology, audio signal processing, and radar signal processing. In 2014, he was a visiting scholar with the Institute of Biomedical Engineering and Technology in Sydney University, Sydney, Australia. In 2019, he was a visiting professor with the department of Electrical and Computer Engineering in University of California, Davis, United States.

Dr. Hong has served as a Steering Committee Member and a TPC Member of the IEEE MTT-S International Microwave Biomedical Conference from 2018 to 2019. He also serves as a member of the IEEE MTT-S Biological Effect and Medical Applications of RF and Microwave (MTT-28). He is an Associate Editor and Guest Editor of the IEEE JOURNAL OF ELECTROMAGNETICS, RF AND MICROWAVES IN MEDICINE AND BIOLOGY.

Changzhi Li (S'06-M'09-SM'13) received the B.S. degree in electrical engineering from Zhejiang University, China, in 2004, and the Ph.D. degree in electrical engineering from the University of Florida, Gainesville, FL, in 2009. He joined Texas Tech University as an Assistant Professor in 2009 and became a Professor in 2020. His research interest is microwave/millimeter-wave sensing for healthcare, security, energy efficiency, structural monitoring, and human-machine interface.

Dr. Li was a recipient of the IEEE Microwave Theory and Techniques Society (MTT-S) Outstanding Young Engineer Award, the IEEE Sensors Council Early Career Technical Achievement Award, the ASEE Frederick Emmons Terman Award, the IEEE-HKN Outstanding Young Professional Award, the NSF Faculty Early CAREER Award, and the IEEE MTT-S Graduate Fellowship Award. He is an Associate Editor of the IEEE TRANSACTIONS ON MICROWAVE THEORY AND TECHNIQUES and the IEEE JOURNAL OF ELECTROMAGNETICS, RF AND MICROWAVES IN MEDICINE AND BIOLOGY.